Inorg. Chem. **2007**, *46*, 5429–5438

Oxo–Molybdenum(VI,V,IV) Complexes of the Facially Coordinating Tris(mercaptoimidazolyl)borate Ligand: Synthesis, Characterization, and Oxygen Atom Transfer Reactivity

Ba L. Tran and Carl J. Carrano*

Department of Chemistry and Biochemistry, San Diego State University, San Diego, California 92182-1030

Received March 19, 2007

A series of monooxo–Mo(IV,V) and dioxo–Mo(VI) complexes of the "soft" tripodal ligand, sodium tris(mercaptoimidazolyl)borate ($NaTm^{Me}$), have been synthesized as potential oxygen atom transfer (OAT) models for sulfite oxidase. Complexes have been characterized by X-ray crystallography, cyclic voltammetry, and EPR, where appropriate. Oxygen atom transfer kinetics of $Tm^{Me}MoO_2Cl$, both stoichiometric and catalytic, have been studied by a combination of UV–vis and ^{31}P NMR spectroscopies under a variety of conditions. OAT rates are consistent with previously established relationships between redox potential/reactivity and mechanistic studies. The analysis of these complexes as potential structural and functional analogues of relevance to molybdoenzymes is further discussed.

Introduction

Metal-catalyzed oxygen atom transfer (OAT) reactions are an important class of chemical transformations, from industrial interest in catalysts derived from Mo, W, and Re to aspects of biological relevance.[1−5] Enzymes containing mononuclear molybdenum and tungsten in their active sites generally catalyze the transfer of an oxygen atom to or from a physiological donor/acceptor with the metal center cycling between the VI and IV oxidation states. The molybdoenzymes are conveniently classified into three main groups, i.e., the xanthine oxidase (XO), dimethyl sulfoxide reductase (DMSOR), and sulfite oxidase (SO) families.[6] Among the three, vertebrate sulfite oxidase (SO) has been extensively investigated due to important biological implications for oxidative degradation pathways involving sulfur containing amino acid residues. Moreover, deficiencies of the enzyme or mutation of the SO structural gene leads to fatal neurological abnormalities directly linked to misregulation and dysfunction in lipid metabolism.[7] Mammalian SO catalyzes the two-electron oxidation of sulfite to sulfate presumably by a process of inner sphere oxygen atom transfer at the molybdenum (VI,IV) center (Scheme 1). The catalytic cycle is completed upon two sequential, coupled, electron−proton transfer (CEPT) steps from the reduced Mo(IV), through an intermediate Mo(V), and finally on to regeneration of the active Mo(VI) oxidized state. The crystal structure of the SO catalytic site confirmed equatorial ligation of a conserved ene-1,2-dithiolate pyranopterin cofactor, an orthogonal thiolate sulfur derived from a protein associated cysteine along with two oxo donors to give a pseudosquare pyramidal Mo(VI) center.[8,9] Hypotheses based on biological and spectroscopic studies suggest that the dithiolene ligation from the pyranopterin cofactor modulates specific reduction−oxidation potentials of the molybdenum center for optimum OAT reactivity and is also critical for electron-transfer regeneration of oxidized SO via a hole superexchange pathway.[10,11] Biochemical site directed mutagenesis has

* To whom correspondence should be addressed. E-mail: carrano@sciences.sdsu.edu.

(1) Enemark, J. H.; Cooney, J. J. A.; Wang, J. J.; Holm, R. H. *Chem. Rev.* **2004**, *104*, 1175−1200.
(2) Ison, E. A.; Corbin, R. A.; Abu-Omar, M. M. *J. Am. Chem. Soc.* **2005**, *127*, 11938−11939.
(3) Ison, E. A.; Trivedi, E. R.; Corbin, R. A.; Abu-Omar, M. M. *J. Am. Chem. Soc.* **2005**, *127*, 15374−15375.
(4) Mitchell, J. M.; Finney, N. S. *J. Am. Chem. Soc.* **2001**, *123*, 862−869.
(5) Wong, Y. L.; Ng, D. K. P.; Lee, H. K. *Inorg. Chem.* **2002**, *41*, 5276−5285.
(6) Hille, R. *Chem. Rev.* **1996**, *96*, 2757−2816.
(7) Garett, R. M.; Johnson, J. L.; Graf, T. N.; Feigenbaum, A.; Rajagopalan, K. V. *Proc. Natl. Acad. Sci. U.S.A.* **1988**, *95*, 6394−6398.
(8) Kisker, C.; Schindelin, H.; Pacheco, A.; Wehbi, W. A.; Garrett, R. M.; Rajagopalan, K. V.; Enemark, J. H.; Rees, D. C. *Cell* **1997**, *91*, 973−983.
(9) Schrader, N.; Fishcer, K.; Theis, K.; Mendel, R. R.; Schawrz, G.; Kisker, C. *Structure* **2003**, *11*, 1251−1263.

10.1021/ic7005259 CCC: $37.00
Published on Web 05/24/2007

Scheme 1. The Catalytic Cycle of the Sulfite Oxidase (SO) Family

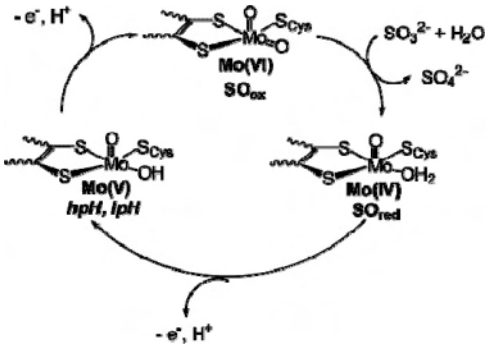

determined that the protein derived cysteine-S ligation is also essential for catalytic competency.

Tripodal tris(pyrazolyl)borate (Tp^R) and tris(pyrazolyl)-methane or "scorpionate" complexes of molybdenum represent a uniquely successful small molecule functional analogue system of molybdo- and tungstoenzymes,[10,12−16] although one would suppose that a symmetric all nitrogen donor ligand would make a poor substitute for the sulfur rich environment relevant to these enzymes. Nevertheless, the Tp^R model remains unmatched by any other system with respect to mimicking the enzymatic OAT catalytic cycle and providing valuable insight into their spectroscopic signatures. Over the last several years, we and others have explored the influence of donor atom identity on OAT reactivity by employing a series of polyfunctional, facially coordinating tridentate N_2X "heteroscorpionate" ligands, in which the third ligating group, X, is readily interchanged between thiolate, phenolate, alkoxide, carboxylate, etc.[17−19] Oxo−molybdenum complexes incorporating these type of ligands are easily synthesized and can exist as two stereoisomers, where the X atom is either cis or trans relative to an oxo group.[20−23] We have demonstrated that both the stereochemistry and the donor atom identity modulate the OAT rates of the complexes based on ligand contributions to the redox potential. However, neither the previously utilized scorpionate nor heteroscorpionate ligands adequately model the sulfur rich coordination site so characteristic of this group of enzymes.

Scheme 2. Overall Synthetic Scheme of Mo(VI,V,IV)−Oxo Complexes of $NaTm^{Me}$

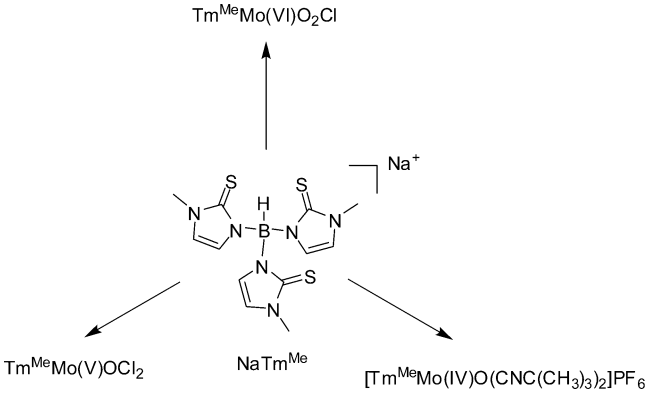

Surprisingly, tris(mercaptoimidazolyl)borate [Tm^{Me}], a "soft" analogue to the popular Tp^R system, although used extensively to model the tetrahedral geometry active sites of zinc enzymes with a sulfur-rich environment, such as the Ada repair protein and liver alcohol dehydrogenase (LADH),[24−27] has never been used to model molybdo- or tungstoenzymes. The facially coordinating three-sulfur donors of the Tm^{Me} ligand are particularly suitable for mimicking the dithiolene and cysteine coordination around the metal center found in sulfite oxidase. Indeed there are very few examples of facial three-sulfur coordinating complexes for molybdenum and tungsten in the literature,[28] two of which are organometallic complexes of Tm^{Me}.[29,30] Therefore we have examined the Tm^{Me} ligand as a potential structural and functional model of molybdoenzyme active site structure using spectroscopy and OAT reactivity. Herein, we report for the first time a series of $Tm^{Me}MoO_2Cl$ (**1**), $Tm^{Me}MoOCl_2$ (**2**), and $[Tm^{Me}MoO(CNC(CH_3)_3)_2]PF_6$ (**3**) complexes along with their complete characterization.

Experimental Section

Synthesis. All syntheses were initially carried out under inert nitrogen atmosphere using standard Schlenk or drybox techniques, while subsequent workups were conducted in air. The reagents, solvents, silica gel 60−200 mesh used in adsorption chromatography, and filtering agent Celite were purchased from the Aldrich Chemical Co. and used as received unless otherwise noted. The sodium salt of the ligand, $NaTm^{Me}$, was synthesized according to a published procedure.[31] The starting material $[Mo(IV)OCl(CNC(CH_3)_3)_4]PF_6$ was prepared based on the literature with little

(10) Inscore, F. E.; McNaughton, R.; Westcott, B. L.; Helton, M. E.; Jones, R.; Dhawan, I. K.; Enemark, J. H.; Kirk, M. L. *Inorg. Chem.* **1999**, *38*, 1401−1410.
(11) Helton, M. E.; Gruhn, N. E.; McNaughton, R. L.; Kirk, M. L. *Inorg. Chem.* **2000**, *39*, 2273−2278.
(12) Xiao, Z.; Young, C. G.; Enemark, J. H.; Wedd, A. G. *J. Am. Chem. Soc.* **1992**, *114*, 9194.
(13) Laughlin, L. J.; Young, C. G. *Inorg. Chem.* **1996**, *35*, 1050−1058.
(14) Smith, P. D.; Millar, A. J.; Young, C. G.; Ghosh, A.; Basu, P. *J. Am. Chem. Soc.* **2000**, *122*, 9298−9299.
(15) Nemykin, V. N.; Davie, S. R.; Mondal, S.; Rubie, N.; Kirk, M. L.; Somogyi, A.; Basu, P. *J. Am. Chem. Soc.* **2002**, *124*, 756−757.
(16) Seymore, S. B.; Brown, S. N. *Inorg. Chem.* **2000**, *39*, 325−332.
(17) Hammes, B. S.; Carrano, C. J. *Dalton Trans.* **2000**, 3304−3309.
(18) Hammes, B. S.; Carrano, C. J. *Inorg. Chem.* **1999**, *38*, 4593−4600.
(19) Otero, A.; Fernandez-Baeza, J.; Antinolo, A.; Tejeda, J.; Lara-Sanchez, A. *Dalton Trans.* **2004**, 1499−1510.
(20) Hammes, B. S.; Chohan, B. S.; Hoffman, J. T.; Einwaechter, S.; Carrano, C. J. *Inorg. Chem.* **2004**, *43*, 7800−7806.
(21) Kail, B.; Nemykin, V. N.; Davie, S. R.; Carrano, C. J.; Hammes, B.; Basu, P. *Inorg. Chem.* **2002**, *41*, 1281−1291.
(22) Davie, S. R.; Rubie, N. D.; Hammes, B. S.; Carrano, C. J.; Kirk, M. L.; Basu, P. *Inorg. Chem.* **2001**, *40*, 2632−2633.
(23) Carrano, C. J.; Chohan, B. S.; Hammes, B. S.; Kail, B. W.; Nemykin, V. N.; Basu, P. *Inorg. Chem.* **2003**, *42*, 5999−6007.
(24) Garner, M.; Reglinski, J.; Cassidy, I.; Spicer, M. D.; Kennedy, A. R. *Chem. Commun.* **1996**, *16*, 1975−1976.
(25) Tesmer, M.; Shu, M.; Vahrenkamp, H. *Inorg. Chem.* **2001**, *40*, 4022−4029.
(26) Ibrahim, M. M.; Seebacher, J.; Steinfeld, G.; Vahrenkamp, H. *Inorg. Chem.* **2005**, *44*, 8531−8538.
(27) Bridgewater, B. M.; Parkin, G. *J. Am. Chem. Soc.* **2000**, *122*, 7140−7141.
(28) Peariso, K.; Chohan, B. S.; Carrano, C. J.; Kirk, M. L. *Inorg. Chem.* **2003**, *42*, 6194−6203.
(29) Foreman, M. R. S. J.; Hill, A. F.; White, A. J. P.; Williams, D. J. *Organometallics* **2003**, *22*, 3831−3840.
(30) Foreman, M. R. S. J.; Hill, A. F.; Tshabang, N.; White, A. J. P.; Williams, D. J. *Organometallics* **2003**, *22*, 5593−5596.
(31) Mihalcik, D. J.; White, J. L.; Tanski, J. M.; Zakharov, L. N.; Yap, G. P. A.; Incarvito, C. D.; Rheingold, A. L.; Rabinovich, D. *Dalton Trans.* **2004**, 1626−1634.

Table 1. Summary of Crystallographic Data and Parameters for [$Tm^{Me}MoO_2Cl$] (**1**), [$Tm^{Me}MoOCl_2$] (**2**·$2CH_2Cl_2$), [$Tm^{Me}MoO(CNC(CH_3)_3)_2]PF_6$ (**3**), and [$Tm^{Me}MoOCl]_2O$ (**4**·3ACN)

	1	**2**	**3**	**4**
molecular formula	$C_{12}H_{16}N_6O_2S_3BClMo$	$C_{26}H_{36}N_{12}O_5S_6B_2Cl_8Mo_2$	$C_{22}H_{34}N_8OS_3BMoPF_6$	$C_{36}H_{32}N_{18}O_3S_6B_2Cl_2Mo_2$
fw	514.70	1286.13	774.47	1241.56
temp (K)	220(2)	200(2)	240(2)	240(2)
cryst syst	monoclinic	triclinic	monoclinic	monoclinic
space group	*Cc*	*P*I	$P2_1/c$	$P2_1/c$
cell constants				
a (Å)	14.7451(8)	9.433(4)	11.5639(15)	9.461(2)
b (Å)	10.6645(8)	14.547(5)	25.181(3)	22.510(5)
c (Å)	12.2089(8)	21.325(8)	12.0206(14)	13.380(3)
α (deg)	90	106.45(2)	90	90
β (deg)	93.575(5)	98.33(2)	99.227(7)	107.334(8)
γ (deg)	90	94.53(2)	90	90
Z	4	2	4	2
V ($Å^3$)	1916.1(2)	2754.7(18)	3455.0(8)	2720.1(11)
abs coeff, μ_{calc} (mm^{-1})	1.171	1.114	0.670	0.842
δ_{calc} (g/cm^3)	1.784	1.551	1.489	1.516
F(000)	1032	1284	1576	1244
cryst dimens (mm^3)	0.2 × 0.2 × 0.1	0.3 × 0.3 × 0.2	0.2 × 0.05 × 0.01	0.2 × 0.05 × 0.02
radiation	Mo Kα	Mo Kα	Mo Kα	Mo Kα
wavelength (Å)	0.710 73	0.710 73	0.710 73	0.710 73
h, *k*, *l* ranges collected	−18 → 22, −16 → 16, −18 → 17	−12 → 12, −18 → 18, −27 → 27	−9 → 9, −19 → 19, −8 → 9	−8 → 8, −20 → 20, −12 → 12
θ range (deg)	2.77−33.22	2.49−27.69	2.36−16.34	2.51−19.53
no. reflns collected	9849	50492	18287	12109
no. unique reflns	6183	12315	1755	2347
no. params	235	551	392	313
data/param ratio	26.3	22.35	4.48	19.75
refinement method	full-matrix least-squares of F^2	full-matrix least-squares of F^2	full-matrix least-squares of F^2	full-matrix least-squares of F^2
$R(F)^a$	0.0378	0.0920	0.0355	0.0422
$R_w(F^2)^b$	0.0849	0.2622	0.0819	0.0957
GOF[c]	0.960	1.062	1.037	1.068
largest diff peak and hole ($e/Å^3$)	0.944 and −0.449	2.779 and −2.362	0.340 and −0.232	0.480 and −0.397

[a] $R = |\Delta F|/|F_o|$. [b] $R_w = w(\Delta F)^2/(wF_o^2)$. [c] Goodness of fit on F^2.

modification[32] as was (py-H)$_2$MoOCl$_5$.[33] The overall synthetic scheme of Mo(IV,V,IV)−oxo complexes of $NaTm^{Me}$ is shown in Scheme 2.

[Tm^{Me}Mo(VI)O_2Cl] (1). To a solution of $NaTm^{Me}$ (513 mg, 1.37 mmol) in MeOH was added dropwise a solution of Mo(VI)O_2Cl_2 (268 mg, 1.35 mmol) in MeOH under nitrogen at ambient temperature. The solution immediately turned bright orange. After stirring for 4 h, an orange solid was collected upon filtration. Yield: 75%. Anal. Calcd for $C_{12}H_{16}N_6S_3O_2BClMo$: C, 28.00; H, 3.13; N, 16.33. Found: C, 28.36; H, 3.34; N, 16.57. ^{1}H NMR (ACN-d_3, 25 °C): *δ* 3.58 (s, 3H, N−C*H*$_3$), 3.59 (s, 3H, N−C*H*$_3$), 3.75 (s, 3H, N−C*H*$_3$), 6.91 (d, 1H, −C*H*−), 6.99 (d, 1H, −C*H*−), 7.05 (d, 1H, −C*H*−), 7.07 (d, 1H, −C*H*−), 7.11 (d, 1H, −C*H*−), 7.24 (d, 1H, −C*H*−). FTIR (KBr, cm^{-1}): *ν* 877, 904 (Mo═O), 2481 (B−H).

[Tm^{Me}Mo(V)OCl_2] (2). Method 1. $MoCl_5$ (183 mg, 0.67 mmol) in a Schenk flask was charged with THF at −78 °C and stirred for 0.5 h producing a brown solution. The sodium salt of the ligand, $NaTm^{Me}$ (250 mg, 0.67 mmol) dissolved in THF at −78 °C, was cannula transferred into the metal solution. After 6 h of stirring, the solvent was removed by vacuum, and the residue was purified by silica gel column chromatography using a 1:1 mixture of acetonitrile/dichloromethane as an eluent. A reddish-brown solid was obtained. Yield: 42%.

Method 2. To a round-bottom flask containing (py−H)$_2$MoOCl$_5$ (500 mg, 1.11 mmol) in 50 mL of ACN was added a solution of $NaTm^{Me}$ (416 mg, 1.11 mmol) dissolved in 75 mL of ACN via a gastight syringe. The solution instantly turned reddish and was stirred overnight under nitrogen. The reddish-brown precipitated product was collected by vacuum filtration and dried under vacuum. Yield: 64%. Anal. Calcd for $C_{12}H_{16}BCl_2MoN_4OS_3 \cdot {}^9/_4CHCl_3$: C, 21.32; H, 2.29; N, 10.47. Found: C, 21.05; H, 2.45; N, 10.82. FTIR (KBr, cm^{-1}): *ν* 933 (Mo═O), 2521 (B−H).

[Tm^{me}Mo(IV)O(CNC(CH$_3$)$_2$)]PF_6 (3). To a solution of $NaTm^{Me}$ (450 mg, 1.20 mmol) in ∼100 mL of ACN was added solid [Mo(IV)OCl(CNC(CH$_3$)$_3$)$_4$]PF_6 (755 mg, 1.20 mmol) leading to a gray colored solution. After 15 min, pyridine was added, and the solution rapidly became dark green. The reaction proceeded overnight under nitrogen atmosphere. The solvent was subsequently removed under vacuum, and the crude product was subjected to column chromatography using dichloromethane as an eluent leading to collection of a dark green band. Precipitation of a green powder was induced by addition of ether to a concentrated dichloromethane solution. The green powder was collected by vacuum filtration, and crystals were obtained by allowing the filtrate to stand. Yield: 35%. Anal. Calcd for $C_{22}H_{34}BF_6MoN_8OPS_3 \cdot C_{10}H_{20}N_2$: C, 40.76; H, 5.78; N, 14.86. Found: C, 40.17; H, 6.13; N, 14.64. FTIR (KBr, cm^{-1}): *ν* 838 (Mo═O), 2162, 2182 (C═N−), 2521 (B−H).

[Tm^{Me}Mo(V)OCl]$_2$O (4). Allowing a solution containing 6.5 mg (1.26×10^{-5} mol) of complex **1** and a 50-fold excess of PPh_3 (165 mg, 6.29×10^{-3} mol) dissolved in a 50:50 v/v mixture of DMSO and acetonitrile (total volume 1 mL) to stand for several days at room temperature resulted in the deposition of small blue-brown crystals which were hand separated and subjected to single-crystal X-ray analysis. They proved to be that of the *μ*-oxo dimer, **4**. The compound was not characterized further.

(32) Novotny, M.; Lippard, S. J. *Inorg. Chem.* **1974**, *13*, 828−831.
(33) Hanson, G. R.; Brunette, A. A.; McDonell, A. C.; Murray, K. S.; Wedd, A. G. *J. Am. Chem. Soc.* **1981**, *103*, 1953−1959.

Table 2. Selected Bond Distances (Å) for [$Tm^{Me}MoO_2Cl$] (**1**), [$Tm^{Me}MoOCl_2$] (**2**), [$Tm^{Me}MoO(CNC(CH_3)_3)_2]PF_6$ (**3**), and [$Tm^{Me}MoOCl]_2O$ (**4**)

	1	2	3	4
Mo(1)−C(13)			2.021(14)	
Mo(1)−C(18)			2.075(15)	
Mo(1)−S(1)	2.651(9)	2.481(2)	2.659(3)	2.709(2)
Mo(1)−S(2)	2.487(9)	2.688(2)	2.438(3)	2.579(2)
Mo(1)−S(3)	2.660(9)	2.506(2)	2.564(3)	2.443(2)
Mo(1)−O(1)	1.736(3)	1.759(6)	1.684(7)	1.8617(8)
Mo(1)−O(2)	1.763(3)			1.669(5)
Mo(1)−Cl(1)	2.357(3)	2.389(3)		2.410(2)
Mo(1)−Cl(2)		2.388(3)		

Table 3. Selected Bond Angles (deg) for [$Tm^{Me}MoO_2Cl$] (**1**), [$Tm^{Me}MoOCl_2$] (**2**), [$Tm^{Me}MoO(CNC(CH_3)_3)]PF_6$ (**3**), and [$Tm^{Me}MoOCl]_2O$ (**4**)

	1	2	3	4
O(1)−Mo(1)−C(13)			95.4(4)	
O(1)−Mo(1)−C(18)			94.0(4)	
C(13)−Mo(1)−C(18)			89.2(4)	
O(1)−Mo(1)−Cl(2)		97.7(2)		
O(1)−Mo(1)−Cl(1)	97.87(10)	98.3(2)		89.58(7)
O(2)−Mo(1)−Cl(1)	100.47(10)			100.7(2)
Cl(2)−Mo(1)−Cl(1)		93.93(10)		
O(1)−Mo(1)−O(2)	105.13(13)			103.7(2)
O(1)−Mo(1)−S(1)	79.77(9)	100.1(2)	167.2(2)	87.70(6)
O(2)−Mo(1)−S(1)	168.14(9)			168.2(2)
C(13)−Mo(1)−S(1)			84.9(4)	
C(18)−Mo(1)−S(1)			73.2(3)	
Cl(2)−Mo(1)−S(1)		162.03(9)		
Cl(1)−Mo(1)−S(1)	89.38(3)	80.85(9)		76.00(8)
O(1)−Mo(1)−S(3)	161.82(9)	88.2(2)	90.6(2)	87.50(6)
O(2)−Mo(1)−S(3)	92.80(10)			99.6(2)
C(13)−Mo(1)−S(3)			173.7(4)	
C(18)−Mo(1)−S(3)			91.9(3)	
Cl(2)−Mo(1)−S(3)		92.36(10)		
Cl(1)−Mo(1)−S(3)	75.48(3)	170.31(8)		159.57(8)
S(1)−Mo(1)−S(3)	83.21(3)	90.93(8)	98.54(10)	83.68(8)
O(1)−Mo(1)−S(2)	99.31(10)	171.9(2)	105.4(2)	174.17(7)
O(2)−Mo(1)−S(2)	82.47(9)			82.1(2)
C(13)−Mo(1)−S(2)			86.3(3)	
C(18)−Mo(1)−S(2)			160.4(3)	
Cl(2)−Mo(1)−S(2)		76.70(8)		
Cl(1)−Mo(1)−S(2)	161.15(3)	88.03(9)		88.86(8)
S(1)−Mo(1)−S(2)	86.10(3)	85.90(8)	87.36(9)	86.47(8)
S(3)−Mo(1)−S(2)	85.82(3)	86.24(8)	90.61(10)	92.01(8)
Mo(1)−O(1)−Mo(1_3)				180.0(3)

Physical Methods. Elemental analysis was performed at Numega Resonance Labs, Inc. (San Diego, CA). ^1H and ^{31}P NMR spectra were recorded on a 500 MHz Varian FT-NMR spectrometer. GC−MS detection of dimethylsulfide was performed on the Varian Chrompack Saturn 2000R GC−MS containing an autosampler operated under the Varian MS Workstation System Control software version 6.6. Electrospray mass spectra (ESI-MS) were recorded on a Finnigan LCQ ion-trap mass spectrometer equipped with an ESI source (Finnigan MAT, San Jose, CA). A PC with Navigator software version 1.2 (Finnigan Corp.) was used for data acquisition and plotting. Isotope distribution patterns were simulated using the program IsoPro 3.0. UV−visible spectra were recorded using a Cary 50 UV−visibility spectrophotometer under PC control using the Cary WinUV software. Infrared spectra were collected on KBr disks on a ThermoNicolet Nexus 670 FT-IR spectrometer under PC control and are reported in wavenumbers. Electrochemical measurements were performed under inert atmosphere at ambient temperature in 0.1 M tetrabutylammonium hexafluorophosphate ($TBAPF_6$) solution as the supporting electrolyte using a BAS Epsilon (Bioanalytical Systems Inc., West Lafayette, IN) voltammetric analyzer. Cyclic voltammetry (CV) employed a three electrode system consisting of glassy-carbon working, platinum wire auxiliary, and Ag/AgCl reference electrodes. The ferrocenium/ferrocene couple was used as an internal standard. Sample solutions were purged with nitrogen, and IR compensation was applied prior to measurements. Isotropic EPR spectra were recorded in dichloromethane solutions at room temperature on a MicroNow 8300A X-band spectrometer operating at approximately 9.38 GHz. Conditions: 3450 G field center, 350 G sweep width, 5.0 G modulation amplitude, 30 s scan time.

OAT Reactivity Studies. A 2.5 mM solution of $Tm^{Me}MoO_2Cl$ in acetonitrile was reacted with an excess of Ph_3P to produce Ph_3PO and $Tm^{Me}MoOCl(ACN)$. The reaction was performed under pseudo-first-order conditions using 25, 50, 75, and 100-fold excess of Ph_3P at 30(1) °C. Fresh samples were prepared for each kinetic run, and solutions were pre-equilibrated at 30 °C in a water bath prior to any measurements. The solvent dependence of OAT reactivity was probed with pyridine, DMF, and THF and ACN. For these experiments a 2.5 mM solution of $Tm^{Me}MoO_2Cl$ in acetonitrile was reacted with a 25-fold excess of PPh_3 in a total volume of 1.0 mL, followed after 5 min by addition of 1.29 mmol of pyridine, DMF, THF, or ACN to the UV−vis quartz cell. Corrections for dilution were made as appropriate.

All reactions were monitored using a Cary 50 UV−vis spectrometer under PC control. Rate constants for OAT were extracted at 740 nm or 500 nm using the scanning kinetics program included with the instrument software. Global fitting of all data was performed with OLIS Spectral Works version 3.0.8 kinetic software.

Catalytic OAT Studies. In a typical experiment, 6.5 mg (1.26×10^{-5} mol) of complex **1** and a 50-fold excess of PPh_3 (165 mg, 6.29×10^{-3} mol) were dissolved in a 50:50 v/v mixture of DMSO and acetonitrile-d_3 with a total volume of 1.0 mL in a NMR tube. The ^{31}P NMR kinetic experiment was performed on a 500 MHz Varian FT-NMR spectrometer with the automated temperature controller set at 30 °C. Prior to kinetic measurements, the NMR sample was equilibrated at 30 °C, and spectra were recorded every 10 min under PC control.

Crystallographic Details. Single crystals suitable for X-ray diffraction structural determination of **1** and **2** were grown by layering a solution of the respective complex in dichloromethane with hexanes at −20 °C. Crystals of **3** were obtained as described in the text, while those of **4** were isolated directly from aged OAT transfer solutions. Crystals of complexes **1**−**4** were attached to nylon loops (Hampton Research) using Paratone oil, frozen in the cold stream of the diffractometer (200−240 K), and mounted on a Bruker X8 APEX CCD diffractometer with a sealed-tube Mo X-ray source. Crystal data collection parameters are summarized in Table 1. The structures were solved by either direct methods or Patterson function, completed by subsequent difference Fourier syntheses, and refined by full-matrix least-squares procedures on F^2. All non-hydrogen atoms were refined with anisotropic displacement coefficients, while hydrogen atoms were treated as idealized contributions using a rigid model except where noted. Selected bond distances and angles for complexes **1**−**4** are depicted in Tables 2 and 3, respectively.

Results and Discussion

Mo(VI) Complex. [$Tm^{Me}MoO_2Cl$] was prepared by a synthetic methodology previously employed for the synthesis of other heteroscorpionate dioxo−molybdenum complexes with little modification. The treatment of $NaTm^{Me}$ with MoO_2Cl_2 in methanol under inert atmosphere precipitated orange solids that were collected by simple filtration in good

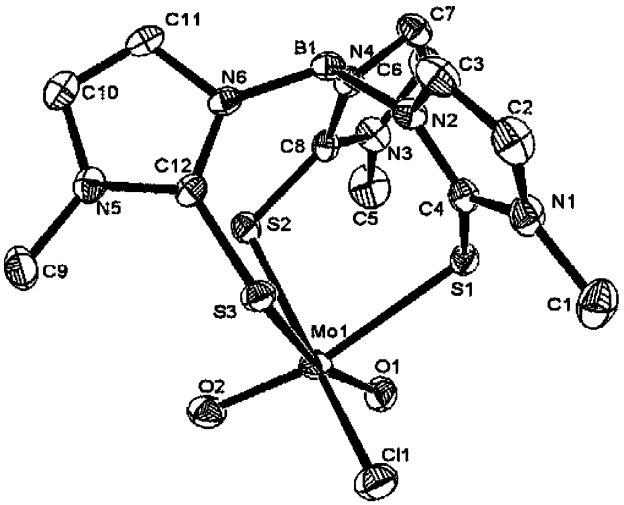

Figure 1. ORTEP diagram with 50% thermal ellipsoids of [$Tm^{Me}MoO_2Cl$] (**1**) showing complete atomic labeling. Hydrogen atoms have been omitted for clarity.

yield. Initial characterization of the isolated solid by IR spectroscopy revealed two intense Mo−oxo stretches at 877 and 904 cm^{-1} and a ν_{B-H} at 2481 cm^{-1} confirming the presence of both metal and ligand. Further characterization of the diamagnetic complex by proton NMR in ACN-d_3 or $CDCl_3$ shows distinct environments for all six of the methimazole protons and all three methyl groups. This is in contrast to what would be expected from the solid-state structure (vide infra) that has local C_{2v} symmetry around the metal and a pseudoplane of symmetry. However, this behavior has been observed before in similar W, Ta, and Nb complexes of this ligand and has been attributed to the intrinsic chirality in the twisted bicyclo[3.3.3]$-C_3-$HB-$(mt)_3$M cages.[29,34]

The X-ray structure for [$Tm^{Me}MoO_2Cl$] (Figure 1) revealed the expected six coordinate structure with the Tm^{Me} sulfur atoms occupying one trigonal face of the octahedron with the two oxo groups and a Cl occupying the other. The two Mo═O bonds are essentially identical and at the expected ∼1.7 Å distance. The S_1 and S_3 atoms, which are each trans to an oxo group, have highly elongated Mo−S bonds (2.65 Å) due to the strong structural trans effect exerted by the latter, while S_2, which is trans to the chloride, exhibits a much shorter metal to sulfur distance of 2.48 Å.

Mo(V) Complexes. Two different synthetic routes have been developed for the formation of [$Tm^{Me}MoOCl_2$] **2**. Reacting $NaTm^{Me}$ with $MoOCl_3(THF)_2$, prepared in situ from a mixture of $MoCl_5$ and THF, afforded a reddish brown solid after column chromatography on silica gel using an acetonitrile/dichloromethane mixture as the mobile phase. Alternatively, we found that treatment of $(py-H)_2MoOCl_5$ with $NaTm^{Me}$ in acetonitrile under nitrogen led to immediate product precipitation from the solution resulting in higher yield and easier access to clean product. Infrared spectra of the two separately prepared products had identical oxo−Mo(V) stretches at 933 cm^{-1}. An isotropic solution

(34) Hill, A. F.; Rae, A. D.; Smith, M. K. *Inorg. Chem.* **2005**, *44*, 7316−7318.

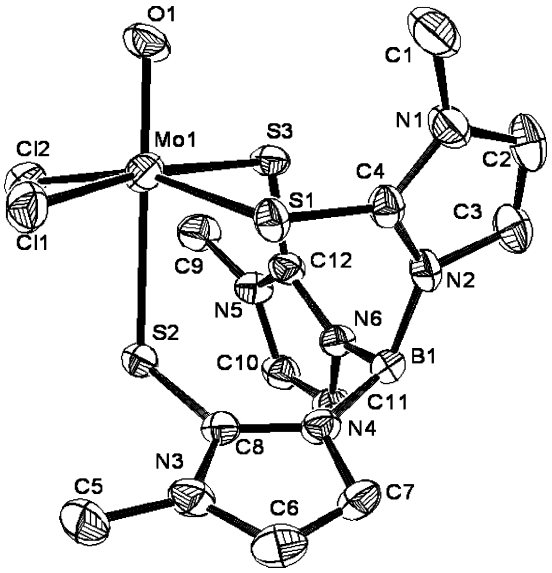

Figure 2. ORTEP diagram with 50% thermal ellipsoids of [$Tm^{Me}MoOCl_2$] (**2**) showing complete atomic labeling. Hydrogen atoms and solvent molecules have been omitted for clarity.

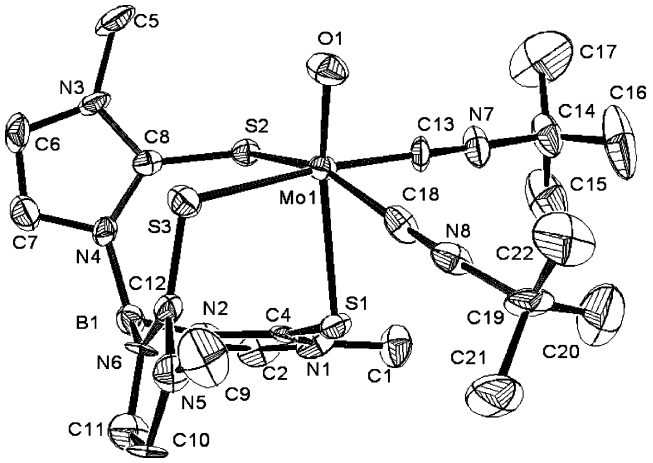

Figure 3. ORTEP diagram with 50% thermal ellipsoids of [$Tm^{Me}MoO(CNC(CH_3)_3)_2]PF_6$ (**3**) showing complete atomic labeling. Hydrogen atoms have been omitted for clarity.

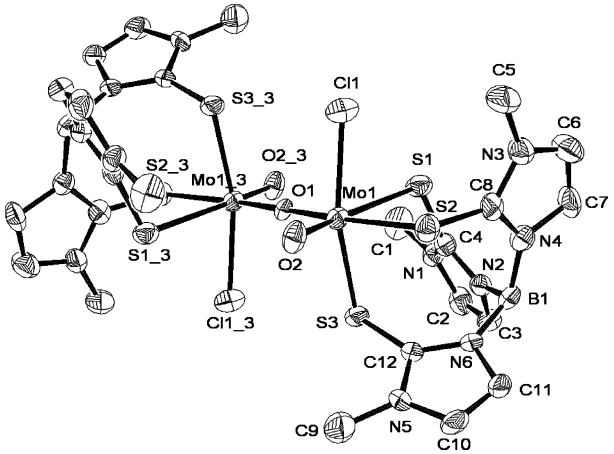

Figure 4. ORTEP diagram with 50% thermal ellipsoids of [$Tm^{Me}MoOCl]_2O$ (**4**) showing partial atomic labeling. Hydrogen atoms and solvent molecules have been omitted for clarity.

EPR spectrum of **2** (Supporting Information) displays the expected ^{98}Mo signal at $g \sim 2$ with six ^{95,97}Mo hyperfine

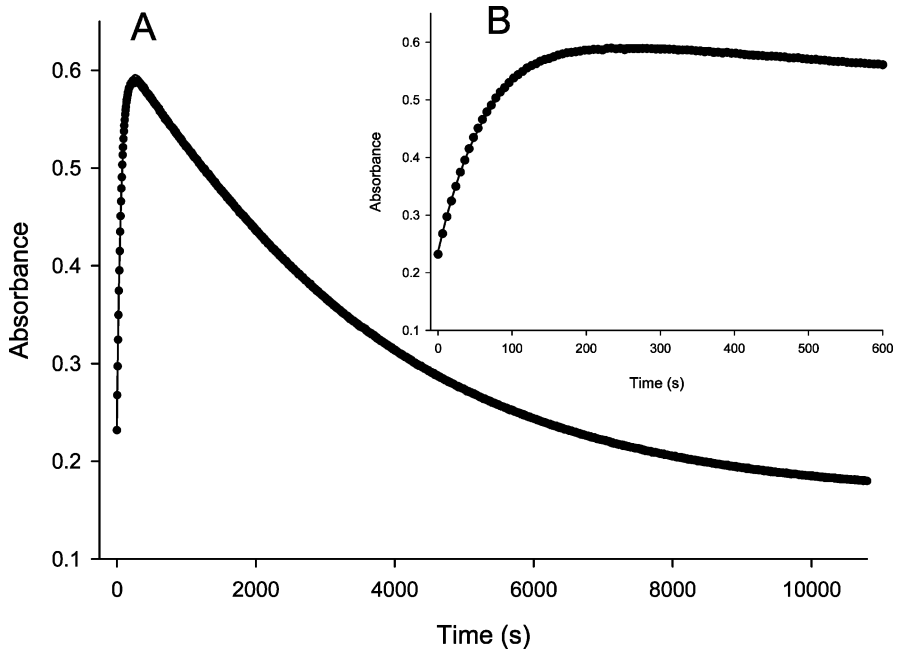

Figure 5. Kinetic plot of the OAT reaction in acetonitrile at 30 °C. The kinetic plot as a function of time (s) was monitored at 740 nm. Plot A shows the complete run, while plot B is a blowup of the first 10 min of the OAT. The points represent the data, and the solid line is a fit to an A → B → C kinetic scheme with rate constants k_1 and k_2.

split lines which define the oxidation state as d^1 Mo(V). The complex is air and water stable for extended periods of time.

The solid-state structure of **2** (Figure 2) reveals that it too adopts a distorted octahedral geometry with two sulfurs and two chlorides orientated opposite to each other in the equatorial plane with Mo−$Cl_{1,2}$ distances of ∼2.38 Å and Mo−$S_{1,3}$ distances of ∼2.5 Å. Because of the strong trans effect of the oxo group, the Mo−S_2 bond trans to it is elongated by 0.20 Å to almost 2.7 Å, which makes the complex functionally a square pyramidal, five coordinate one.

Mo(IV) Complex. Generally, isolation of reduced mononooxo−Mo(IV) complexes is achieved indirectly through transfer of an oxygen atom from dioxo−Mo(VI) complexes to a PR_3 acceptor, in a donor solvent such as pyridine, acetonitrile, or dimethylformamide. Here however we have synthesized the oxo−Mo(IV) complex directly by overnight reaction of [Mo(IV)OCl(CNC$(CH_3)_3)_4$]PF_6 and $NaTm^{Me}$ in acetonitrile under a dry nitrogen atmosphere.

Single-crystal X-ray diffraction studies of the extremely thin green needles required extensive integration times, and even so the resulting structure is not of as high a quality as the other two complexes. Nevertheless all the salient structural features are revealed (Figure 3). The complex itself is monocationic, with a single well-ordered hexafluorophosphate anion in the unit cell. The three sulfurs of the ligand again occupy one trigonal face of the octahedron with the lone oxo group and two neutral *tert*-butylisonitriles occupying the other. The Mo(IV)═O bond is slightly shorter, 1.684 Å, than that seen in the corresponding neutral Mo(V) and (VI) complexes, presumably due to the cationic nature of the metal fragment. Once again, the S_1−Mo bond, situated trans to the oxo atom, is the most elongated at 2.66 Å. The other two Mo−S bonds, each of which is trans to an isonitrile, average 2.5 Å. The complex is unusual in terms of its charge, since rather than achieving electroneutrality by retaining a chloro ligand in the primary coordination sphere as we almost invariably see with these types of complexes, the metal center incorporates two neutral monodentate *tert*-butylisonitriles, thereby generating a mononuclear cationic species. It is clear the Tm^{Me} ligand is capable of stabilizing the otherwise air-sensitive oxo−Mo(IV) state from oxidation as crystals retained their color and morphology over several days in air. Thus, [Tm^{Me}MoO(CNC$(CH_3)_3)_2$]PF_6 may serve as a potentially useful synthon via substitution chemistry of the two labile *tert*-butylisonitrile ligands.

***μ*-Oxo Dimer.** In addition to the mononuclear species described above, we have detected the presence of a dinuclear species by single-crystal diffraction. This observation is however a common feature in oxo−molybdenum chemistry. The *μ*-oxo dimer (Figure 4) consists of two distorted octahedral Tm^{Me}MoO(V)Cl units bridged by an oxo group. The two chlorides and Mo═O groups are oriented trans to each other with typical bond lengths for Mo−Cl at 2.41 Å and Mo═O at 1.67 Å. The bridging Mo−O1 bond length of 1.86 Å is consistent with single bond character for an oxo donor. The Mo−O−Mo unit is completely linear with a 180° bond angle. The Mo−S distances are similar to the other Mo complexes reported here. Charge considerations make this a Mo(V)/(V) dimer which could be formed either by comproportionation of the Mo(IV) complex produced by OAT transfer with unreacted Mo(VI) or by hydrolysis of any of the mononuclear species followed by appropriate redox chemistry.

Electrochemistry. Cyclic voltammetry of **1** in dichloromethane displayed only one irreversible cathodic wave at $E_{1/2} = -0.80$ V for the one-electron reduction to Mo(V).

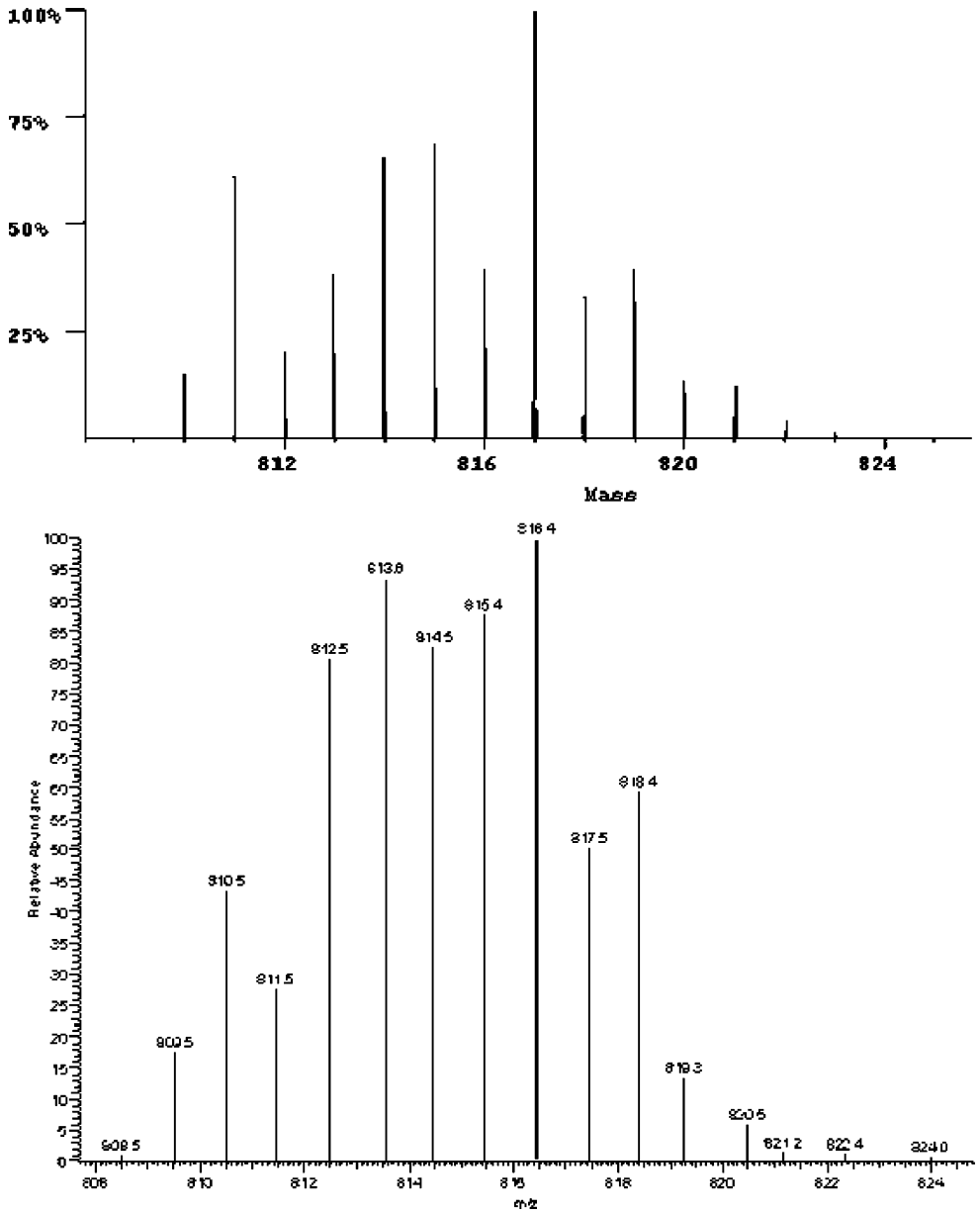

Figure 6. The calculated isotope pattern (above) for $[KTm^{Me}MoOCl(OPPh_3)]^+$. Below is the experimental isotope pattern determined by positive ion mode ESI-MS in acetonitrile.

The irreversibility indicates that the analogous $[MoO_2]^+$ species cannot be stabilized or a dimerization process prevents regeneration of the dioxo−Mo(VI) complex. The reduction potential of $Tm^{Me}MoO_2Cl$ is more negative than that of $Tp^{Me}MoO_2Cl$ by approximately 0.13 V. Among the series of heteroscorpionate complexes, only the sulfur containing $(L3S)MoO_2Cl$ seems comparable to **1** with an $E_{1/2} = -0.83$ V.[20]

Cyclic voltammetric examination of $Tm^{Me}MoOCl_2$ showed two largely irreversible processes with $E_{1/2} = -0.63$ V for the reductive Mo(IV/V) couple and $E_{1/2} = +1.22$ V for the oxidative Mo(V/VI). The potential difference between the two redox processes of 1.85 V is similar to reported values.[23] Previously, we reported the electrochemical behavior of $(L3S)MoO(SPh)_2$ and $(L3S)MoO(bdt)_2$, both of which show quasireversible waves for both the reduction of Mo(V) to Mo(IV) between −0.35 and −0.45 V and the oxidation of Mo(V) to Mo(VI) in the +0.60 to +0.80 V range.[28] Complex **2** showed a largely irreversible one-electron reduction and is harder to reduce by ∼180 mV. Likely, this is due to the fact that sulfur donors of the Tm^{Me} ligand are formally neutral thiones rather than true anionic thiolates.

OAT. To mimic substrate oxidation catalyzed by molybdoenzymes, we have measured the kinetics of OAT between complex **1** and PPh_3 under pseudo- first-order conditions. The course of the OAT reaction was followed by electronic spectroscopy using either the appearance of an intense band at 500 nm or the weak broad band in the 600−900 nm region where the d−d transitions of oxo−Mo(IV) product species generally appear.[35,36] The OAT reaction proceeded smoothly in acetonitrile, in which initial isobestic

(35) Roberts, S. A.; Young, C. G.; Kipke, C. A.; Cleland, W. E.; Yamanouchi, K.; Carducci, M. D.; Enemark, J. H. *Inorg. Chem.* **1990**, *29*, 3650.

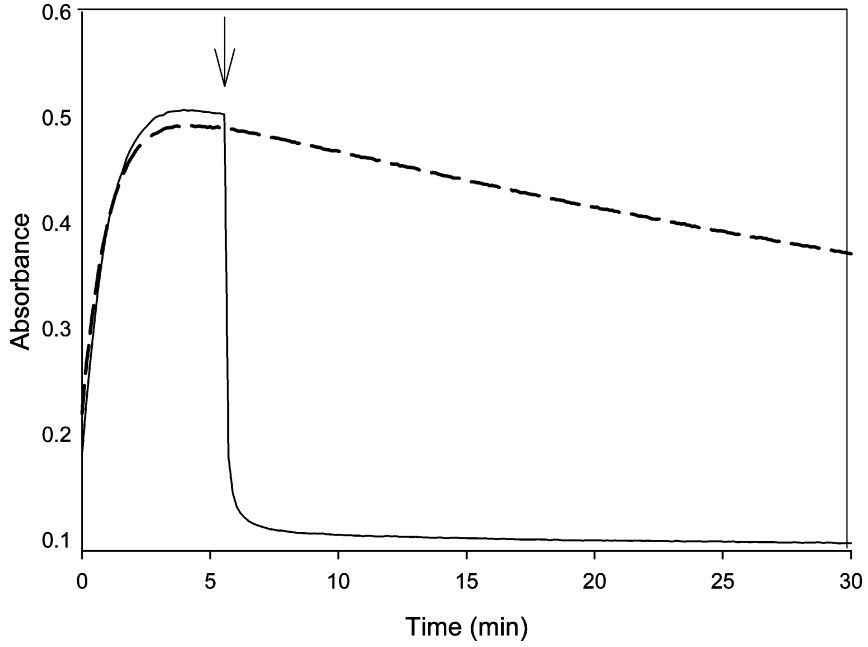

Figure 7. An absorbance vs time plot for the OAT reaction between $Tm^{Me}MoO_2Cl$ and triphenylphosphine in pure acetonitrile (− − −) and in the presence of pyridine (—). The arrow indicates the point of addition of pyridine to the acetonitrile solution.

behavior was observed at 425 nm. The overall reaction however was clearly biphasic with an initial rapid exponential growth of both the 500 and the 600−900 nm features followed by a much slower reduction in intensity of these bands (Figure 5). These data could be adequately fit assuming a sequential A → B → C reaction mechanism. We postulate that the first rapid process represents an oxygen atom transfer from complex **1** to produce the phosphine oxide adduct. This reaction is linearly dependent on the concentration of triphenylphosphine and yields a second-order rate constant of $k_1 = 1.94 \times 10^{-1}$ M^{-1} s^{-1} at 30 °C (Supporting Information). The measured OAT rate for $Tm^{Me}MoO_2Cl$ is consistent with the published relationship between the redox potential and OAT where $TpMoO_2Cl$ > $Tm^{Me}MoO_2Cl$ > $(L3S)MoO_2Cl$ as expected.[20]

The detection of the coordinated phosphine oxide adduct by ^{31}P NMR at both low temperature (−30 °C) and 30 °C is consistent with the hypothesis that the first kinetic process is the two-electron reduction of the Mo(VI). The complex $Tm^{Me}MoOCl(OPPh_3)$ appears at 45 ppm while free $OPPh_3$ resonates at 27 ppm in this system and PPh_3 at −5 ppm. After elevation of the temperature of sample to 40 °C for 4 h, the peak attributed to $Tm^{Me}MoOCl(OPPh_3)$ disappeared with a concomitant growth in the peak belonging to free $OPPh_3$, which correlates well with the OAT reactivity as monitored by electronic spectroscopy. The presence of Tm^{Me}-$MoOCl(OPPh_3)$ was further confirmed by positive ion ESI-MS in acetonitrile, where an ion cluster consistent with $[KTm^{Me}MoOCl(OPPh)_3]^+$ was observed (Figure 6).

Recently, Young, Basu, and co-workers have isolated and completely physically characterized the phosphine oxide adducts $Tp^RMoOCl(OPR_3)$ and $Tp^RMoO(OPh)(OPR_3)$ as intermediates in the OAT process.[14,37−40] These phosphine oxide bound species were proposed to subsequently break down via a dissociative process to yield a solvated Mo(IV) complex of the form Tp^RMoOCl(solvent). Detailed theoretical calculations also supported a mechanism of OAT involving initial formation of a phosphine oxide bound intermediate via an associative process followed by dissociative loss of the phosphine oxide and subsequent solvation.[41] In accordance with literature we therefore identified the second slow kinetic process we observe as the dissociative loss of the phosphine oxide and the formation of the solvated species $Tm^{Me}MoOCl$(solvent).

Although the measured entropy of activation for the formation of Tp^RMoOX(solvent) from $Tp^RMoOX(OPR_3)$ determined by Basu et al. clearly revealed a generally dissociative mechanism, neither experimental nor theoretical calculations offered a clear distinction between a purely dissociative pathway and the corresponding dissociative interchange, I_d, one. In the latter case, the Mo−solvent bond formation must begin before the Mo−OPR_3 bond is completely broken, and the metal center never becomes truly pentacoordinate as in the pure dissociative pathway. However, unlike the case reported by Young and Basu where the rate of solvation was the same in both ACN and THF, the second kinetic step in our system shows a significant solvent dependence.

To probe the effect of solvent on the displacement of $OPPh_3$ from the intermediate, we monitored the rate of the

(36) Roberts, S. A.; Young, C. G.; Cleland, W. E.; Ortega, R. B.; Enemark, J. H. *Inorg. Chem.* **1988**, *27*, 3044−3051.

(37) Nemykin, V. N.; Laskin, J.; Basu, P. *J. Am. Chem. Soc.* **2004**, *126*, 8604−8605.

(38) Nemykin, V. N.; Basu, P. *Inorg. Chem.* **2005**, *44*, 7494−7502.

(39) Millar, A. J.; Doonan, C. J.; Smith, P. D.; Nemykin, V. N.; Basu, P.; Young, C. G. *Chem.—Eur. J.* **2005**, *11*, 3255−3267.

(40) Kail, B. W.; Perez, L. M.; Zaric, S. D.; Millar, A. J.; Young, C. G.; Hall, M. B.; Basu, P. *Chem.—Eur. J.* **2006**, *12*, 7501−7509.

(41) Pietsch, M. A.; Hall, M. B. *Inorg. Chem.* **1996**, *35*, 1273−1278.

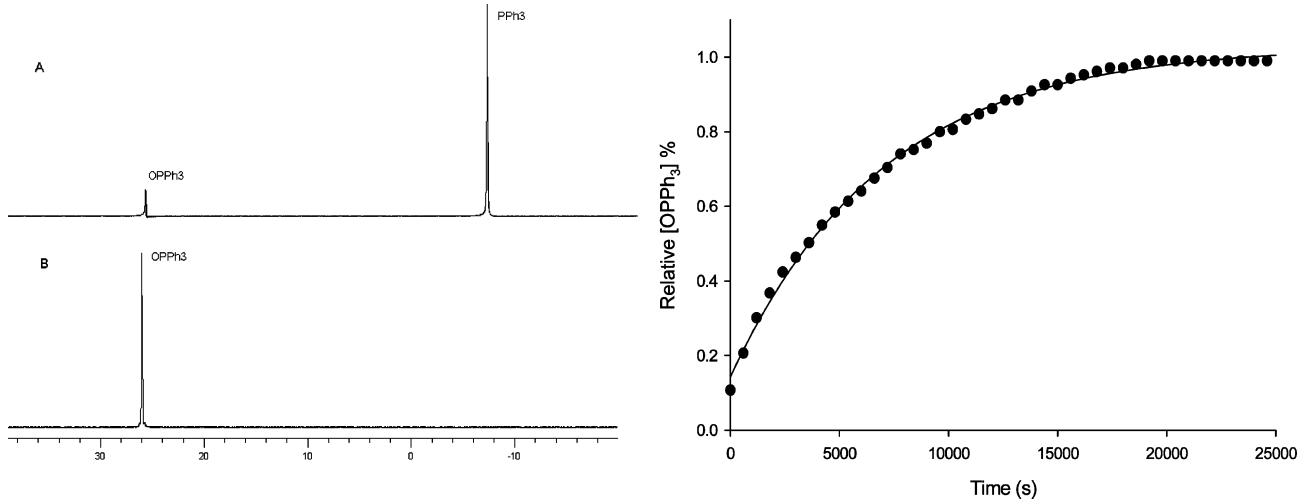

Figure 8. ^{31}P NMR spectra (left) obtained during catalytic oxidation of PPh_3 (−5 ppm) to $OPPh_3$ (27 ppm): (A) initial scan; (B) after complete conversion (∼5 h). The growth of $OPPh_3$ as a function of time is also presented to the right.

decay of the coordinated phosphine oxide adduct in the presence of solvents of varying donor ability (pyridine, DMF, THF, and ACN) by UV−vis spectroscopy. In these experiments, the $Tm^{Me}MoO_2Cl$ complex and triphenylphosphine where mixed in acetonitrile. After the rapid formation of the phosphine oxide adduct, the solution was allowed to age for approximately 5 min at 30 °C to establish a base rate of solvation by ACN. At the 5 min point, an aliquot of an alternate solvent was added and the change in rate measured. As can be seen from Figure 7, the addition of pyridine, a strong donor solvent, leads to a rapid reaction to form what we believe to be $Tm^{Me}MoOCl(py)$. The relative order of reactivity follows: pyridine ≫ DMF > THF ≈ ACN. Since the reaction with pyridine is too fast to measure under our conditions and THF is not very different from acetonitrile, we studied the solvation by DMF in more detail. The results indicate DMF promotes $OPPh_3$ release much more effectively than either THF or ACN in a concentration dependent fashion (Supporting Information). Thus a plot of k_{obs} vs [DMF] is linear with a nonzero intercept on the *y*-axis, the intercept being the rate of solvation by the bulk acetonitrile. Together these observations support the notion of a solvent assisted dissociative interchange mechanism for the breakdown of the phosphine oxide adduct rather than a simple pure dissociative loss of $OPPh_3$ from the primary coordination sphere.

Catalytic Oxidation of PPh_3 with DMSO. The assessment of $Tm^{Me}MoO_2Cl$ for catalytic oxidation of PPh_3 was performed in 50:50 v/v DMSO and acetonitrile at 30 °C in the presence of a 50-fold excess of the phosphine. The reaction was monitored by the appearance of $OPPh_3$ (27 ppm) as probed by ^{31}P NMR (Figure 8). Complete conversion of PPh_3 to $OPPh_3$ product was observed within ∼5 h with $k_{obs} = 1.54 \times 10^{-4}$ s^{-1} under these conditions. In a control experiment, without adding complex **1** only trace amounts of $OPPh_3$ were detected after 24 h due to phosphine reacting with atmospheric oxygen. In a separate experiment, after complete conversion of a 50-fold excess of PPh_3 to $OPPh_3$, the catalytic cycle could be reinitiated by addition of more PPh_3, suggesting the catalyst is regenerated and remains

Scheme 3. The Proposed Pathway for Oxygen Atom Transfer between DMSO and PPh_3 Catalyzed by Complex **1**

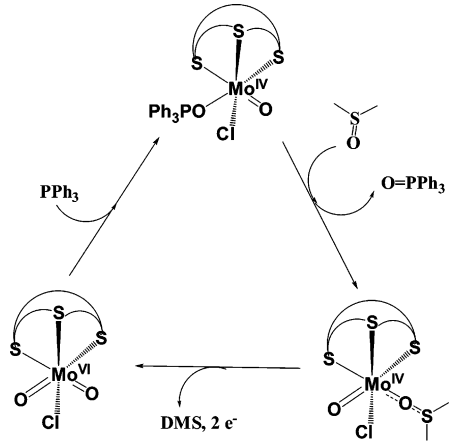

1

active. It is possible to follow the progress of the reaction visually as the initially yellow solution becomes deep red on addition of the phosphine and then gradually turns green. The return of the yellow color indicates regeneration of the active species after the consumption of all the triphenylphosphine. We speculate that the green solution indicates the binding of DMSO to the $Mo^{IV}O$ center leading back to OAT and regeneration to the starting $Mo^{VI}O_2$ complex. Scheme 3 shows the proposed catalytic cycle of the oxygen atom transfer from complex **1** to phosphine with DMSO as the oxygen donor. The existence of dimethyl sulfide was confirmed by GC−MS. Addition of an aliquot of the good donor solvent, pyridine, to the reaction medium completely deactivates the catalytic cycle as determined by ^{31}P NMR. Presumably the strong coordination by pyridine to the vacant site at the metal center after OAT prevents binding and subsequent oxo atom abstraction from DMSO inhibiting the regeneration of $Tm^{Me}MoO_2Cl$, and thus no catalytic turnover is observed.

The identity of the active catalyst in these systems is subject to some uncertainty given the isolation of the μ-oxo dimer, **4**, from aged reaction mixtures. However the observed 1:1 rather than 2:1 stoichiometry between $Tm^{Me}MoO_2Cl$ and

triphenylphosphine required for complete OAT as determined by ^{31}P NMR in acetonitrile strongly favors the mononuclear complex as the active catalyst. The isolation of the μ-oxo−Mo(V/V) dimer is likely the result of either slow hydrolysis or a comproportionation reaction between some of the initially formed Mo(IV) species with unreacted dioxo−Mo(VI). Overall, this system represents an example of a relatively rare class of functional analogues capable of achieving catalytic activity reminiscent of mononuclear molybdenum enzymes but is unique in more closely mimicking their coordination environment.[35,36,42,43]

Conclusion

We have isolated and physically characterized complexes of tris(mercaptoimidazolyl)borate [Tm^{Me}] in all three oxo−Mo oxidation states postulated to be important in the OAT catalytic cycle of molybdoenzymes. The dioxo−Mo(VI) complex mimics enzymatic OAT functionality by oxidation of triphenylphosphine in acetonitrile, whose rate follows the reported redox potential trend. The complex also exhibited catalytic oxidation of PPh_3 into $OPPh_3$ with DMSO as the oxygen donor in acetonitrile at 30 °C, while at the same time the sulfur rich environment of Tm^{Me} has more resemblance to mononuclear Mo active sites than the all nitrogen coordination of Tp^R.

Note Added in Proof. While this work was under review, the structure of **1** and its reactivity with sulfite were reported. The results of the two studies are complementary.[44]

Acknowledgment. This work was supported in part by NSF Grant CHE-0313865 (C.J.C.). The NSF-MRI Grant CHE-0320848 is acknowledged for support of the X-ray diffraction facilities at San Diego State University.

Supporting Information Available: Additional crystallographic data (files in CIF format) for **1**−**4**, EPR spectrum of **2**, and k_{1obs} vs [PPh_3] and k_{2obs} vs [DMF] kinetic plots. This material is free of charge via the Internet at http://pubs.acs.org.

IC7005259

(42) Holm, R. H.; Berg, J. M. *Acc. Chem. Res.* **1986**, *19*, 363−370.
(43) Berg, J. M.; Holm, R. H. *J. Am. Chem. Soc.* **1985**, *107*, 925−932.
(44) Wallace, D.; Gibson, L. T.; Reglinski, J.; Spicer, M. D. *Inorg. Chem.* [Online early access]. DOI: 10.1021/ic700468m. Published Online: April 10, 2007.